Proceedings of the 8th International Congress on Thermal Stresses, TS2009
1–4 June, University of Illinois at Urbana-Champaign

Towards A Continuum Multiphysics Simulation of Metal Solidification Processes

Seid Koric[1] Brian G. Thomas[2] and Rui Liu[2]

[1] *National Center for Supercomputing Applications-NCSA, University of Illinois Urbana-Champaign, USA*

[2] *Department of Mechanical Science & Engineering, University of Illinois at Urbana-Champaign, USA*

A coupled computational thermo-mechanical model has been developed to simulate the continuous casting of complex shaped sections, such as used for steel beam blanks. An efficient numerical procedure to integrate the constitutive equations at the local level is combined with a global finite-element solution of temperature and stress. It includes realistic constitutive behavior of the liquid/mushy zone, delta-ferrite, and austenite phases of the solidifying steel shell using a fixed grid approach. Heat transfer is computed in the shell, the complex-shaped mold, and across the interfacial gap between them, and is fully-coupled with the stress model to include the effect of shell shrinkage and gap formation on lowering the heat flux. Current work, to incorporate results from turbulent thermal-fluid flow simulations of liquid pool into this thermal-stress model, is introduced.

Key Words: *Solidification, Finite-Element, Abaqus, Thermal-Stress, Fluid Flow, Superheat*

1 Introduction

Many manufacturing and fabrication processes such as foundry shape casting, continuous casting and welding have common solidification phenomena. One of the most important and complex of these is continuous casting, which produces 90% of steel today. Even though the process is constantly improving, there is still a significant need to minimize defects and to maximize quality and efficiency.

The high cost of plant experiments under the harsh operating steel plant conditions makes it appropriate to develop computational models that can predict temperature, deformation, and stress in the solidifying steel shell in the mold during continuous casting of near-net-shape sections with sufficient accuracy to solve practical problems such as the design of mold taper, and optimization of fluid flow to avoid cracks.

Numerical modeling of the thermo-mechanical solidification of the shell presents a large number of computational difficulties, such as the integration of the highly nonlinear visco-plastic constitutive laws, treatment of liquid/mushy zone, treatment of superheat fluxes coming from turbulent fluid flow in liquid pool, treatment of latent heat, accounting for the temperature dependence of material properties, contact between the solidified shell and mold surfaces, and coupling between the heat transfer and stress analysis.

This work uses the method developed by Koric et al Ref.[1] who implemented a robust local viscoplastic integration schemes from an in-house code CON2D Ref.[2] into the commercial finite element package Abaqus Ref.[3] via its user defined material subroutine UMAT including the special treatment of liquid/mushy zone.

2 Governing Equations, Solutions Procedures, and Validation of Thermal-Stress Model

The transient energy equation is given in Eq. (1):

$$\rho\left(\frac{\partial \mathbf{H}(\mathbf{T})}{\partial \mathbf{t}}\right) = \nabla \cdot \mathbf{k}(\mathbf{T})\nabla \mathbf{T} \qquad (1)$$

along with boundary conditions of prescribed temperature, prescribed heat flux, or the following practical convection condition:

$$-\mathbf{k}\nabla \mathbf{T} \cdot \mathbf{n} = \mathbf{h}_g(\mathbf{T} - \mathbf{T}_m) \qquad (2)$$

where ρ is density, k is isotropic temperature-dependent thermal conductivity, H is temperature-dependent enthalpy including latent heat of solidification, h_g is an effective heat transfer coefficient, T_m is the mold surface temperature, and **n** is the unit vector normal to the boundary.

Inertial effects are negligible in solidification problems, so using the static mechanical equilibrium in Eq. 3 as the governing equation is appropriate

$$\nabla \cdot \boldsymbol{\sigma}(\mathbf{x}) + \mathbf{b} = 0 \qquad (3)$$

where σ is the Cauchy stress tensor, and **b** is the body force density vector.

The rate representation of total strain in this elastic-viscoplastic model is given by Eq. (4):

$$\dot{\boldsymbol{\varepsilon}} = \dot{\boldsymbol{\varepsilon}}_{el} + \dot{\boldsymbol{\varepsilon}}_{ie} + \dot{\boldsymbol{\varepsilon}}_{th} \tag{4}$$

where $\dot{\boldsymbol{\varepsilon}}_{el}, \dot{\boldsymbol{\varepsilon}}_{ie}, \dot{\boldsymbol{\varepsilon}}_{th}$ are the elastic, inelastic, and thermal strain rate tensors respectively.

Viscoplastic strain includes both strain-rate independent plasticity and time dependant creep. Creep is significant at the high temperatures of the solidification processes and is indistinguishable from plastic strain. Kozlowski at al Ref.[4] proposed a unified formulation with the following functional form to define inelastic strain.

$$\dot{\bar{\varepsilon}}_{ie}[\sec^{-1}] = f_C \left[\bar{\sigma}[MPa] - f_1 \bar{\varepsilon}_{ie}\right]^{f2-1} \bar{\varepsilon}_{ie}^{\,f3} \exp\left(-\frac{Q}{T[K]}\right)$$

where :

$$Q = 44,465$$

$$f_1 = 130.5 - 5.128 \times 10^{-3} T[K]$$

$$f_2 = -0.6289 + 1.114 \times 10^{-3} T[K] \tag{5}$$

$$f_3 = 8.132 - 1.54 \times 10^{-3} T[K]$$

$$f_C = 46,550 + 71,400\,(\%C) + 12,000\,(\%C)^2$$

Q is activation constant, and f_1, f_2, f_3, f_C are empirical temperature, and steel-grade-dependant constants. Another constitutive law, the modified power-constitutive model developed by Zhu Ref.[2], is used to simulate the delta-ferrite phase, which exhibits significantly higher creep rates and lower strength than the austenite phase.

The system of ordinary differential equations defined at each material point by the viscoplastic model equations is converted into two "integrated" scalar equations by the backward-Euler method and then solved using a special bounded Newton-Raphson method Ref.[1] in user subroutine UMAT.

Abaqus main code is using the fully implicit staggered coupled algorithm for time integration of the governing equations Ref. [3]. In each time step the thermal field is solved, and then the resulting thermal strains are used to solve the mechanical problem. Newton-Raphson iteration continues until tolerances for both equation systems are satisfied before proceeding to the next time step.

The solidification stress model used in this work was validated by comparison with a semi-analytical solution of thermal stress in an unconstrained solidifying plate Ref.[5]. Fig. 1 shows the stress distributions, across the solidifying shell at two different times and compares the semi-analytical solution with the numerical solutions from both Abaqus and CON2D codes. The thermal stress results match very well among all three methods. More details about this validation can be found in Ref.[1].

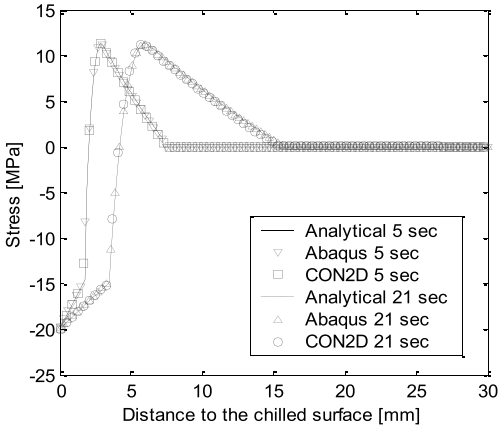

Fig. 1 Thermal Stress Numerical Validation

3 Thermo-Mechanical Model of Beam Blank Casting

The computational model solves the coupled temperature, stress and deformation in a beam blank caster known for its complex geometry. Fig. 2 shows a schematic of a cross section of the beam blank caster normal to the casting direction. The mold has cooling channels at the outer edge of the mold. The generalized plane strain finite element domain is used in this work in Lagrangian frame of reference as it moves down the cast. It encompasses ¼ of the section with a slice of a simplified mold wall (neglecting the internal water slots) and the corresponding "stripe" of the strand adjacent to the mold wall, which is wide enough to allow solidification of expected shell thickens everywhere. This avoids expensive computation in the large liquid domain and contributes to significant cpu time saving and also to the robustness of the model.

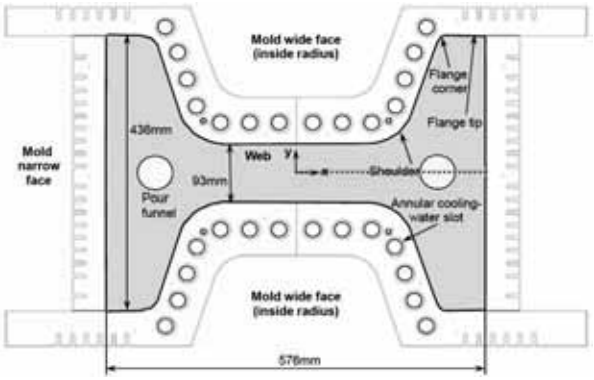

Fig. 2 Schematic of a transverse BB cross section

Temperature dependent properties Ref.[1] were chosen for 0.071 %C plain carbon steel with Tsol=1471.9 C and Tliq=1518.7 C. Those include: enthalpy, thermal conductivity, thermal expansion, and

elastic modulus. In addition to Kozlowski III model from Eq. 6, the delta-phase model is applied in the solid whenever the volume fraction of ferrite is more than 10%. The calculation of the volume fractions of the liquid, delta, and austenite phases is an integral part of UMAT subroutine.

The shape of the distorted mold wall is computed using 3-D elastic thermal stress analysis of ¼ of the entire copper mold plates and steel backing plates and water jacket structure.

Two way thermal-mechanical coupling in needed in this model since the stress analysis is dependant on temperature distribution through thermal strains, while the heat conducted between mold and strand depends strongly on distance between separated surfaces and is calculated from mechanical solution. The gap heat transfer coefficient hg is found according to:

$$\begin{aligned} h_g &= h_o && d \le d_0 \\ h_g &= \frac{1}{\frac{d}{k_{air}} + R_c} + h_{rad} && d_0 < d \end{aligned} \qquad (6)$$

where d is the gap size, d_0 is the critical gap size (taken to be 0.1 mm in this work), k_{air} is the thermal conductivity of the gas in the gap, R_c is the contact resistance of the interface, h_{rad} is the effective heat transfer coefficient due to radiation, and h_0 is the gap heat transfer coefficient corresponding to a gap of size d_0. Values of these terms, which vary with temperature, and further details of this gap heat transfer calculation are given elsewhere Ref.[2].

By describing the displacements of the mold contact surface with respect to the time bellow meniscus the actual mold taper used in the plant to compensate for shell shrinkage is modeled.

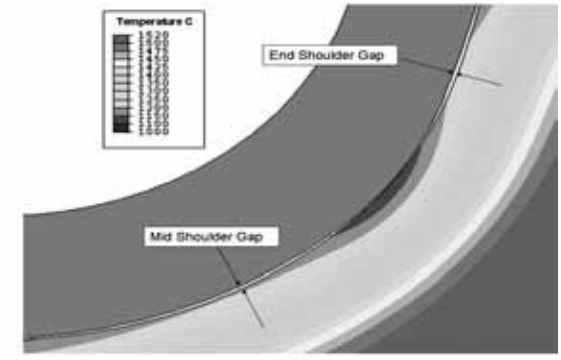

Fig. 3 Beam-Blank Shoulder shell temperature contour with gap details

The shoulder region of beam-blank mold in Fig 3. has a convex shape which is opposite to the corners. Heat extraction in shoulder is therefore retarded, yielding a thinner shell with higher temperature. Presence of a gap in the middle shoulder indicates a bending of the shell caused by pressure exerted by the middle area of the flange. Another small gap is present at the end of the shoulder arch, and is mainly generated by the mold curvature change.

The maximum and minimum principal stress contours at 457 mm shell breakout distance from plant measurement are given in Fig. 4. They reveal expected compressive shell behavior at the "cold" surface and tensile stress in the hot interior near the solidification front, similar to the model validation from Fig 1. Maximum stress and strain is found in the shoulder area which is not a surprise since the thinner shell in this region caused by gap formation leads to stress concentration. Longitudinal cracks and breakouts are often found in this same shoulder region, as revealed by plant observations.

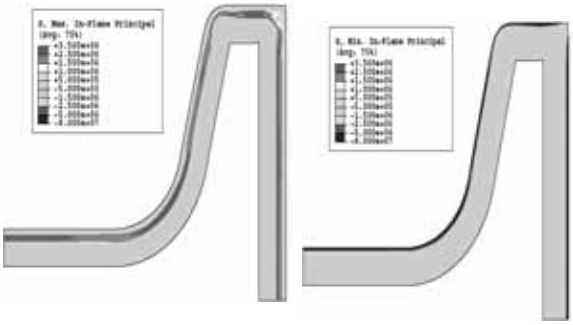

Fig. 4 Max. and Min. Minimum principal stress contour 457 mm below meniscus

Shell thickness at 30% solid from this model is compared with the measured shell breakout data in Fig. 5. A good match is observed everywhere except the middle portion of the wide face where the measured shell appears to be 5 mm thicker. This is likely caused by the uneven superheat distribution due to the flow pattern in the liquid pool. Therefore, there is a growing need to include the effects of fluid flow into a thermal stress analysis. The ongoing multiphysics work to model all 3 phenomena (fluid flow, heat transfer, and stress) is briefly outlined in the next 2 chapters.

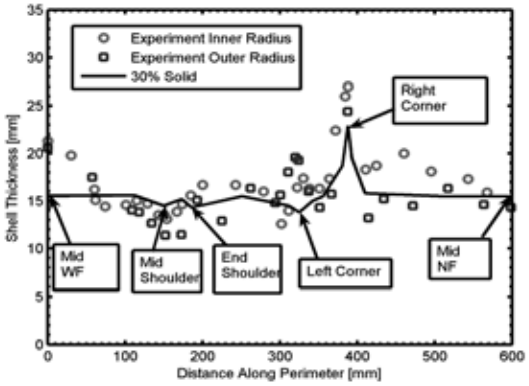

Fig. 5 Shell thickness comparisons 457 mm below meniscus

4 Heat and Fluid-Flow Analysis of Liquid Pool

Fluid flow in the liquid pool controls the distribution of superheat to the inside surface of the solidifying shell. The 3-D velocity field is calculated

by solving the turbulent Navier-Stokes equations with the k-ε model in FLUENT. The domain is the liquid pool and is curved according to known shape of the solid shell. It extends to the liquidus surface, which has vertical downward velocity fixed at the casting speed. This condition is incorporated as mass and momentum sinks, in order to use standard wall laws [Ref. 6].

Fluid enters through a funnel which catches the gravity-drivent stream from the tundish bottom. This is represented with a fixed-velocity, K, and ε inlet boundary plane. Typical results in Fig. 6 show that with a reasonably tight stream, the jet penetrates deep into the liquid pool. A strong recirculation region forms, bringing liquid up the centerline in the mold.

The heat transport equation is then solved in the liquid pool for the accompanying superheat distribution and heat flux to the shell boundary, $q^*_{sup.ht}$. The typical temperature contours in Fig. 6 (right) show that the hot jet (red) delivers its maximum heat to the shell where it impinges tangentially part way down the mold. The rest of the top surface is relatively cold, including the web region where the shell grows thickest.

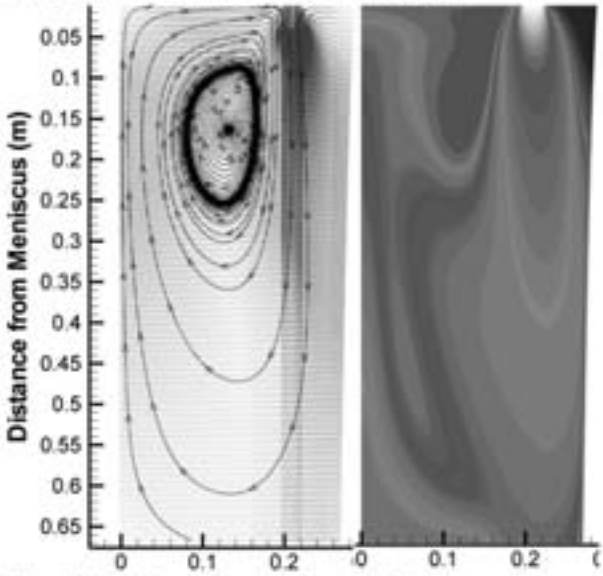

Fig. 6 Velocities and streamlines (left) and temperature contours (right) in centerplane of liquid pool

5 Incorporating Superheat Effects into Thermo-Mechanical Model via Enhanced Latent Heat

Fluid flow causes shell thinning and temperature changes which affect the thermal stress behavior. The multiphysics approach of simulating all 3 phenomena (fluid flow, heat transfer, and stress) simultaneously is very computationally demanding and requires oversimplification of the individual phenomena. A more accurate approach is to decouple the fluid flow simulation from the thermal stress analysis, if the liquid pool shape can be determined a-priori. In many processes that involve a stable interface shape, such as cryolite ledge formation, or the continuous casting of steel, this is relatively easy to do. A new method is being developed to incorporate the effects of heat transfer in the liquid pool into simulations of solidification in the mushy and solid regions.

Computational results of fluid flow and heat transfer in a liquid domain can be characterized by the heat flux crossing the boundary representing the solidification front, or liquidus temperature. This "superheat flux" can be incorporated into a simulation of heat transfer phenomena in the mushy and solid regions, by enhancing the latent heat. Starting with the Stefan interface condition, the additional latent heat to account for superheat flux delivered from liquid pool can be calculated from Eq. (7).

$$\Delta H_f = \frac{q^*_{sup.ht}}{\rho_s \, v} \tag{7}$$

where v is the instantaneous interface velocity which can be estimated from analytical or numerical solutions.

A user subroutine UMATHT Ref.[3] was created to implement the enhanced latent heat method into Abaqus. The focus of current work is to include superheat results from fluid flow analysis from section 4 into the coupled thermo-mechanical model of beam blank by linking both mechanical (UMAT) and thermal (UMATHT) user subroutines with Abaqus. This is an efficient and accurate way to achieve multiphysics simulations of metal solidification on continuum level.

Acknowledgment

The authors would like to thank the Steel Dynamics Structural and Rail Mill, Continuous Casting Consortium at the University of Illinois, the National Science Foundation Grant # DMI 05-28668, and NCSA for computational and software resources.

References

(1) S. Koric and B.G. Thomas, Efficient Thermo-Mechanical Model for Solidification Processes, International Journal for Num. Methods in Eng. Vol. **66** 1955-1989, 2006

(2) Zhu H., Coupled thermal-mechanical FE model with application to initial solidification, Ph.D. Thesis, University of Illinois 1993

(3) Abaqus User's Manual 6.8, Dassault Sys., 2008

(4) P.F. Kozlowski, B.G. Thomas, J.A. Azzi, and H. Wang, Simple constitutive equations for steel at high temperature, Met. Mat. Tran. A, Vol. 23, 903-918, 1992

(5) J.H. Weiner and B.A. Boley, Elastic-plastic thermal stresses in a solidifying body, J. Mech. Phys. Solids, Vol. **11** 145-154, 1963

(6) B. Rietow, MS Thesis, U. Illinois, 2007.